Rheol Acta 35:417–432 (1996)

ORIGINAL CONTRIBUTION

H. Martin Laun
Claudius Kormann
Norbert Willenbacher

Rheometry on magnetorheological (MR) fluids

I. steady shear flow in stationary magnetic fields

Received: 21 June 1996
Accepted: 27 August 1996

Dr. H.M. Laun (✉) · Dr. C. Kormann
Dr. N. Willenbacher
BASF Aktiengesellschaft
Polymer Research Laboratory
ZKM-G209
67056 Ludwigshafen/Rhein, Germany

Abstract Test fixtures of a commercial concentric cylinder rheometer (Physica Rheolab MC 20) were modified to enable measurements under magnetic inductions up to 0.5 Tesla in a shear rate range of 0.1 up to 1000 s^{-1} and temperatures 0° to 150°C. In the 2×90°-cups only two 90° sectors of the stationary part of the double concentric cylinder arrangement are submitted to the magnetic field which is created outside the test tools by an electromagnet. A prototype of a 360°-cup contains the electromagnet within the cup and avoids the correction necessary for the sector geometry. Measurements are shown for a carbonyl iron MR fluid and two nano MR fluids. An encouraging comparison of the viscosity function and MR effect (shear stress changes due to the field) measured by using the various cups is presented. The detailed investigation of the magnetic field distribution in the tools yields a distinct radial field gradient and also stray fields that make the quantification of the effective field in the gap difficult. The change of the field when the gap is filled with MR fluid is addressed. MR effects up to 13000 Pa have been found, the limited torque range of the rheometer making it necessary to use relatively small gap dimensions which introduce errors due to edge effects. Shear rates up to 40000 s^{-1} as typical for the application in dampers were investigated by a piston-driven capillary rheometer making use of a thermostated rectangular slit with superimposed magnetic field. A satisfactory agreement of the magnetorheological data with the concentric cylinder results is found in the overlapping shear rate range.

Key words Magnetorheology – NMR fluids – cencentric cylinder rheometry – slit die theometry – distribution of magnetic field

Introduction

Magnetorheological (MR) fluids have stimulated considerable activities in recent years because of potential applications in controllable shock absorbers, clutches, engine mounts, precision linear drives and other systems (Hartsock et al., 1991; Carlson, 1994; Tönshoff and Stegmann, 1995). While a great variety of MR fluid systems have been described there still remains a need for reliable measurement methods and apparatuses that work under conditions close to the situation in practical devices, i.e. high energy dissipation. Little experience is available on the compatibility of data obtained from one type of rheometer with data from another rheometer. We present in this study data from various experimental set-ups using different measurement geometries thus allowing to judge the reliability of the results. Potential sources of errors are addressed and recommendations given. In this part, we concentrate on steady-state flows under stationary magnetic

Rheologica Acta, Vol. 35, No. 5 (1996)
© Steinkopff Verlag 1996

fields oriented perpendicular to the plane of shear. The second part (Laun et al., 1996) will be devoted to oscillatory shear and/or alternating magnetic fields.

Literature review on methods and materials

A variety of apparatuses is found in the literature for studying the viscosity of MR fluid systems: Weser and Stierstadt (1985) used a viscobalance based on a ball being drawn through a tube. A concentric-cylinder rotational viscometer was adopted by Kamiyama et al. (1987). Kashevskii et al. (1990) studied the relaxation of viscous stresses in magnetorheological suspensions using a hydraulic piston operated rheometer. A plate-plate geometry inserted into a coil was used by Lemaire and Bossis (1991) and Minagawa et al. (1994). Principles of the proper application of rotational viscometers were discussed by Janocha and Rech (1994). Weiss et al. (1994) have characterized the yield stress of ER and MR fluids by using a stress controlled rotational rheometer in oscillatory mode.

Since the early work on MR fluids by Rabinow (1949) where carbonyl iron particles with diameter in the μm range suspended in oil were used, several other MR fluid systems were described: Mixtures of monodisperse polystyrene spheres (μm diameter) with ferrofluids (Skjeltorp, 1984) colloidal suspensions of polystyrene particles (diameter 0.8 μm) containing Fe_3O_4 inclusions (Lemaire and Bossis, 1991), and suspensions of polymer-coated nano-sized ferrite particles (diameter ≈ 0.03 μm) in polar solvents (Kormann et al., 1994; BASF 1995). One should also mention here conventional ferrofluids that yield, however, only rather small viscosity changes in magnetic fields (Rosensweig et al., 1969; Weser and Stierstadt, 1985; Ambacher et al., 1992). Some systems were designed to show viscosity changes in both magnetic and electric fields (Kordonsky et al., 1994; Minagawa et al., 1994).

Theoretical work

Several papers were published exploring the potential of magneto- (and electro-) rheological systems: Rosensweig (1995) calculated the yield stress from a continuum model of asymmetric stress states that occur when a material becomes anisotropic (e.g., segregates into microscopic laminae or columns) under the influence of a field. Ginder et al. (1995) use a finite element analysis to calculate the field distribution in chains of magnetizable particles and describe the maximum yield stress as a function of volume fraction and saturation magnetization of the magnetic particles in the MR fluid. Another particle chain model is described by Lemaire et al. (1995) who take into consideration the Brownian motion of particles as a function of particle size. These models are quasi static and do not consider the hydrodynamic interactions of sheared suspensions due to the solvent. A dynamic model for the yield stress under shear was derived for electrorheological (ER) fluids (cf. section III in Bonnecaze and Brady (1992). Hess et al. (1990, 1993) used non-equilibrium molecular dynamics (NEMD) computer simulations to study the anisotropy of the viscosity and the particle structures of a "gas" of magnetic particles.

MR effect and viscosity ratio

The shear stress and viscosity measured for a given shear rate $\dot{\gamma}$ without superimposed magnetic field are denoted as $\tau(0)$ and $\eta(0)$, respectively. To quantify magnetic fields in the rheometer we use throughout this paper the magnetic induction B. For a definition of the induction or magnetic flux density and its relation to other magnetic quantities see Appendix II. At constant shear rate an imposed magnetic induction B yields a shear stress $\tau(B)$ and viscosity $\eta(B)$. The shear stress increase $\Delta\tau(B)$ due to the field is called the MR effect:

$$\Delta\tau(B) \equiv \tau(B) - \tau(0) = \dot{\gamma}\,[\eta(B) - \eta(0)] \quad \text{for } \dot{\gamma} = \text{const} \tag{1}$$

The viscosity ratio $\eta_r(B)$ defines the factor of the viscosity increase with regard to the field free state:

$$\eta_r(B) \equiv \frac{\eta(B)}{\eta(0)} = \frac{\tau(B)}{\tau(0)} \quad \text{for } \dot{\gamma} = \text{const} \tag{2}$$

It depends on the application which of the two properties are more relevant. Since it is in general desirable to reach high transmittable shear stresses in the fluid the MR effect is the quantity mostly focused on. Note that η_r is defined for a given shear rate. Much higher relative viscosities may be obtained if values measured at a given shear stress are considered.

Energy dissipation

Most studies on MR and ER fluids make use of commercial rheometers (e.g., with cone-plate or Couette geometry) that were modified to impose a magnetic or electric field, respectively. Therefore, parameters like the maximum attainable shear rate or shear stress are limited by the design of the rheometer. In a practical device, like a controllable shock absorber, clutch, etc., a considerable amount of energy needs to be dissipated within a relatively small volume of the fluid. Typical values for the desired power consumption are $N = 100-5000$ W in a volume of $V = 1-20$ cm^3 thus yielding a power density $P = N/V$

which is orders of magnitude higher than what can be achieved in conventional rotational rheometers. Typical values for P are $1-3\cdot10^8$ W/m^3. The power density is related to the shear rate $\dot\gamma$ and shear stresses τ by

$$P=\eta\dot\gamma^2=\tau\dot\gamma\ , \tag{3}$$

η being the viscosity. Typical values for the shear stress $\tau(B)$ are in the range of 4–10 kPa. Since τ is essentially limited by the fluid performance the necessary power dissipation has to be achieved by using shear rates in the range of several 10^4 s^{-1}. The resulting high shear rates are hardly accessible by rotational rheometers. Rather, capillary rheometry has to be used to extend the shear rate range up to 10^5 s^{-1}.

Modes of operation

In the area of fluids with externally controllable viscosity it is common to denote as shear mode the drag flow between (at least in flow direction) parallel walls that are displaced relative to each other at a velocity v, F being the resulting force (Fig. 1a). For an area $b\cdot l$ and wall distance h the shear stress τ and shear rate $\dot\gamma$ follow as

$$\tau=\frac{F}{bl} \tag{4}$$

and

$$\dot\gamma=\frac{v}{h}\ . \tag{5}$$

The second type of deformation is the so-called valve mode (or flow mode) which denotes the extrusion through a parallel slit (Fig. 1b). For an rectangular slit of width h and breadth b a flow rate Q gives rise to an (apparent) wall shear rate

$$\dot\gamma=\frac{6Q}{bh^2}\ . \tag{6}$$

being correct for a Newtonian fluid. For non-Newtonian MR fluids the true wall shear rate may be determined from the apparent flow curve by application of the Rabinowitch-Weissenberg correction. We will restrict ourselves to apparent values in this paper, however. From the pressure along a extrusion length l follows the true wall shear stress as

$$\tau=\frac{p}{2l/h}\ . \tag{7}$$

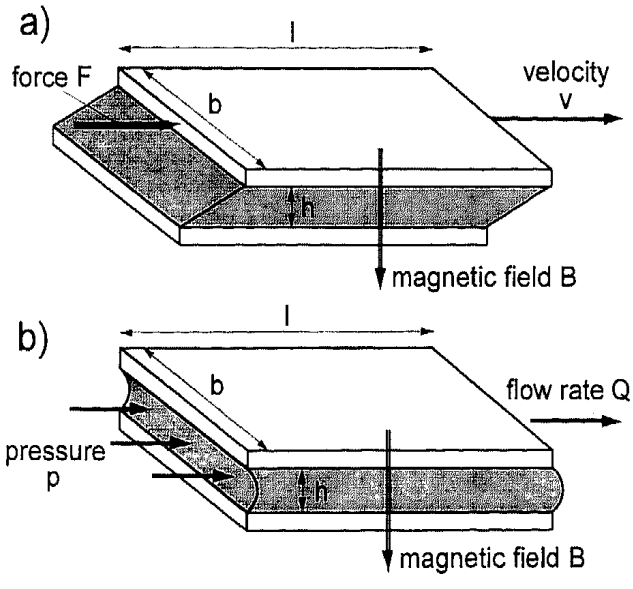

Fig. 1 Shear mode (a) and valve mode (b) of an MR fluid (schematic)

Samples

Experimental results are presented for three samples A, B, and C which are characterized in Table 1. Sample A is a carbonyl iron MR fluid with µm particles, whereas samples B and C represent nano MR fluids (Kormann et al., 1994) of different solid content. Due to the high density of the ferrite ($\varrho=5.0-5.2$ g/cm^3) a weight concentration of 60% corresponds to a ferrite volume concentration of 23%. The true hydrodynamic volume concentration of the particles is higher due to the effect of a stabilizing polymer layer on the particle surface. It is, however, outside the topic of this paper to discuss details of the sample composition and its relation with the resulting MR effect.

Table 1 Magnetorheological fluids investigated in this study

Sample	Particle type	Saturation magnetization [T]	Content of magnetic material [%] by weight
A	carbonyl iron, µm-sized	0.20	≈55
B	ferrite, nano-sized	0.13	≈60
C	ferrite, nano-sized	0.14	≈70

Double concentric cylinder viscometer

The 2×90° geometry (shear mode)

For Couette type steady shear measurements we have modified the test fixtures of a Physica Rheolab MC 20 rheometer to impose a magnetic field perpendicular to the plane of shear. This is depicted in Fig. 2 for the

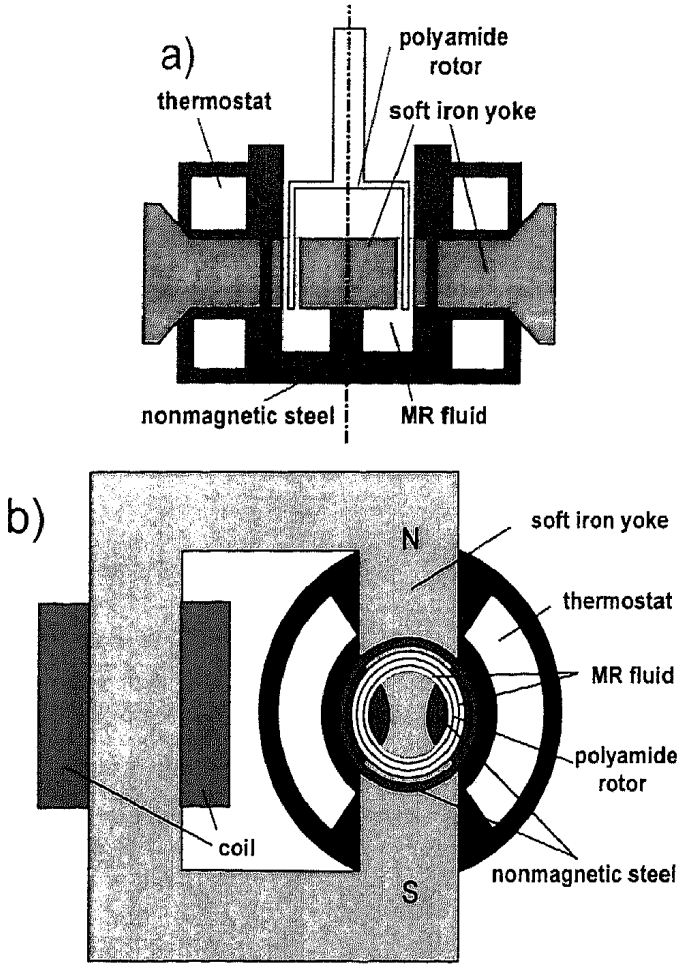

Fig. 2 Side view (a) and top view (b) of the double concentric cylinder viscometer with 2×90° geometry (schematic)

2×90° geometry. The measuring unit is mounted in a standard cup of the rheometer thus simplifying replacement of the MR-fixtures and making use of the thermostat of the instrument. By using glycol as the thermostat fluid a temperature range of 0° to 150 °C could be covered.

The MR-cup is stationary and contains a soft iron yoke to guide the magnetic flux. The MR fluid contained in an annular gap is sheared between the moving rotor and the stationary yoke. To avoid eddy currents the rotor is made of polyamide (an investigation whether the polyamide wall might introduce slip effects of the MR samples is outside the topic of this paper). The drive unit of the rheometer imposes a torque on the rotor and measures the resulting speed of rotation. An electromagnet located outside the cup creates the magnetic induction. The top view of the arrangements shows that only two 90° sectors of the central stationary cylinder in the cup consist of soft iron, whereas the rest of the cylinder is made of non magnetic steel. Due to this geometry only two 90° sectors of the sample are submitted to a radial magnetic flux. The other half of the sample is in principle field free (details to be discussed below).

Note that depending on the radial position in the shear gap the volume elements of the MR fluid rotate at angular speeds ranging from zero up to the angular frequency of the rotor. As a consequence the rotating elements experience in the 2×90° geometry for measurements with imposed magnetic induction a pulsating field strength. As long as the characteristic time for the build-up and decay of the field-induced structures in the sample is small compared to the reciprocal of the pulsation frequency no effect due to the pulsation is to be expected. For long switching times, however, this may cause an error compared to a stationary field. This issue will further be addressed in the second part of the paper.

The 360° geometry (shear mode)

Recently, a prototype of a 360° test fixture was developed (cup DS05EB3). Figure 3 shows a schematic drawing of the cross-section. Here the electromagnet is contained in the cup. The design is completely axisymmetric. The radii of the annular gap correspond to that of the smaller 2×90° cup (compare Table 2). We have a radial magnetic flux throughout the whole gap of the yoke. This avoids the additional correction step which is necessary for the 2×90° geometry when an external field is applied (see below). The path of the magnetic flux is much shorter compared to the arrangement in Fig. 1. However, the given dimensions of the standard Physica cup limits the size of the coil. In order to reach the desired magnetic induction it may be necessary to use high currents that give rise to resistive heating of the coil. Another factor to be addressed is the saturation magnetization of the central magnetic rod the diameter of which must be smaller than that of the annular gap in the yoke. The yoke of the cur-

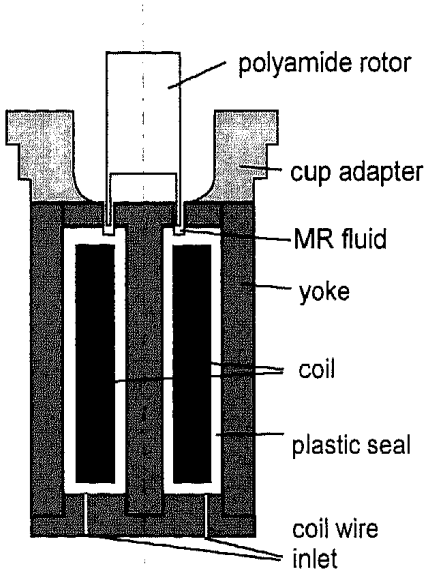

Fig. 3 Side view of the double concentric cylinder viscometer with 360° geometry (schematic)

Table 2 Geometry and nominal range of the 2×90°-cups DS20EB1 and DS09EB2 and the 360°-cup DS05EB3

Property	Symbol	Dimension	DS20EB1	DS09EB2	DS05EB3
Inner radius gap 1	R_{i1}	mm	15.00	8.00	8.00
Outer radius gap 1	R_{o1}	mm	16.10	8.58	8.58
Gap width 1	ΔR_1	mm	1.10	0.58	0.58
Inner radius gap 2	R_{i2}	mm	19.40	9.00	9.00
Outer radius gap 2	R_{o2}	mm	21.00	9.95	9.95
Gap width 2	ΔR_2	mm	1.60	0.85	0.85
Gap height	H	mm	20	9.0	5.0
Max. rotary speed	n_{max}	rpm	800	800	800
Max. angular velocity	Ω_{max}	rad/s	83.7	83.7	83.7
Max. shear rate	$\dot{\gamma}$	s^{-1}	1120	1110	1110
Shear rate ratio	$\dot{\gamma}_1/\dot{\gamma}_2$		1.04	0.99	0.99
Max. torque	M_{max}	Nm	0.05	0.05	0.05
Max. shear stress	τ_{max}	Pa	626	5125	9225

rent prototype consists of soft iron. By replacing iron e.g. by Vacoflux 50 (Vacuumschmelze Hanau) and optimizing details of the yoke geometry it is hoped to distinctly improve the performance of the 360° test fixture.

Geometrical consideration

The double concentric cylinder geometry is schematically depicted in Fig. 4. For simplicity we select the gap dimensions such that the shear rates for a Newtonian fluid are the same on both sides of the rotor wall (see Appendix I). In addition the dimensions are such that these shear rates correspond to that of the Physica Z-cup ($\beta = 0.850$), Ω standing for the angular velocity:

$$\dot{\gamma} = \frac{2\Omega}{1-\beta} \quad \beta \equiv \left(\frac{R_{i2}}{R_{o2}}\right)^2 . \tag{8}$$

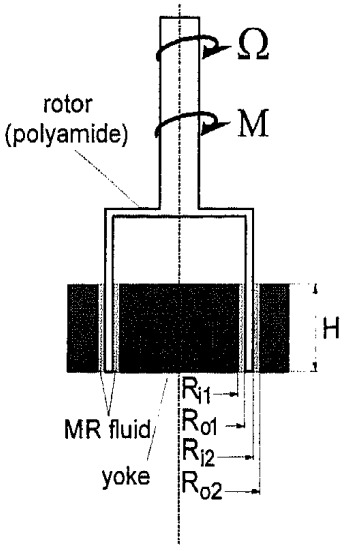

Fig. 4 Schematic of the double concentric cylinder arrangement

This choice is of advantage to avoid rescaling of the Physica Rheolab MC 20 shear rate reading. The shear stress τ follows from the measured torque M (see Appendix I) as

$$\tau = \frac{M}{2\pi H(R_{o1}^2 + R_{i2}^2)} . \tag{9}$$

Table 2 lists the geometrical details of three test fixtures that have been designed to meet this condition. Note that for a non-Newtonian fluid both $\dot{\gamma}$ and τ represent apparent values. We do not apply pertinent corrections to extract true values since the apparent values seem sufficient for the practical purposes under consideration.

Since the maximal torque and rotary speed of the instrument are given the attainable shear stresses and shear rates may be calculated from the above equations (compare Table 2). Cup DS20EB1 is a 2×90°-cup with a rotor diameter of 40 mm and a gap height of 20 mm to be used for fluids with low MR effect (max. 626 Pa). To extend the shear stress range to 5000 Pa we have used cup DS09EB2 with only 9 mm gap height and 20 mm rotor diameter. Due to the relatively small gap width it is more difficult to assure the concentricity of rotor and annular gap. All test fixtures have been calibrated by using the PTB calibration oil 10000 A (viscosity 7.911 Pa·s at 20 °C). If necessary, the effective rotor height H_{eff} was adjusted to obtain the correct viscosity. It should also be mentioned that the maximum torques given in Table 2 for the 2×90 geometry refer to a Newtonian fluid. According to Eq. (11) the value for MR-fluids under field may be up to a factor 2 higher.

A further increase of the attainable shear stress may be achieved by emerging the rotor only in part into the gap, e.g. by H/2 or H/3. The rheometer readout for the viscosity has then to be corrected by a factor 2 or 3, respectively. Practically, the height variation is done during a continuous measurement of the torque such that the rheometer

Rheologica Acta, Vol. 35, No. 5 (1996)
© Steinkopff Verlag 1996

readout enables a direct control of the torque variation. Note that end effects may cause non-negligible errors in this case.

Evaluation of MR fluid viscosity and MR effect

For the 360°-cup the rheometer readout at a given shear rate directly gives the values $\tau(B)$ or $\eta(B)$, respectively. To predict damper characteristics one may wish to describe the experimental data by a fit-function. For this purpose a generalized Bingham-Casson law is pertinent:

$$\tau(\dot{\gamma}) = [\tau_0^n + (\eta_\infty \dot{\gamma})^n]^{1/n} \quad . \tag{10}$$

Note that the three parameters τ_0 (apparent yield stress), η_∞ (high shear viscosity) and n (exponent, $0<n<1$) are depending on the magnetic induction.

For the 2×90°-cup only half of the shear plane is submitted to the magnetic flux. For measurements under field, the rheometer reading represents an apparent shear stress $\tilde{\tau}(B)$,

$$\tilde{\tau}(B) = \frac{\tau(B)+\tau(0)}{2} \tag{11}$$

or apparent viscosity $\tilde{\eta}(B) = \tilde{\tau}(B)/\dot{\gamma}$, respectively. Here, the true shear stress $\tau(B)$ follows from the relation

$$\tau(B) = 2\tilde{\tau}(B) - \tau(0) \quad \text{for } \dot{\gamma} = \text{const} \quad . \tag{12}$$

Practically, the zero field data $\tau(0,\dot{\gamma})$ are fitted by Eq. (10) which yields the parameters $\tau_0(0)$, $\eta_\infty(0)$ and $n(0)$. With the help of the zero field fit function the shear rate dependent apparent shear stress is now converted into the true values $\tau(B,\dot{\gamma})$ using Eq. (12). Taking benefit of the zero field fit, it is not necessary to have the measurements with magnetic flux done at exactly the same shear rates. If the resulting flow curve is again fitted by Eq. (10) the parameters $\tau_0(B)$, $\eta_\infty(B)$ and $n(B)$ are obtained.

Experimental examples for the 2×90° geometry

Figure 5 demonstrates the procedure for the carbonyl iron MR fluid A at 80 °C. The zero field data (full diamonds) are approximated by the zero field fit (broken line, $\tau_0(0) = 30$ Pa, $\eta_\infty(0) = 1.9\cdot10^{-7}$ Pa s, $n(0) = 0.157$). The typical shear thinning behavior of a concentrated suspension is found.

The unfilled triangles represent the apparent viscosity $\tilde{\eta}$ from the rheometer under field (magnetic induction $B^* = 0.2$ T). The latter viscosity is converted into the true viscosity (full squares). The full line represents a fit of the viscosity function with field, the parameters being $\tau_0(B) = 920$ Pa, $\eta_\infty(B) = 1.0\cdot10^{-4}$ Pa s, $n(B) = 0.145$. Note that the dominant effect of the field is an increase of the apparent yield stress, whereas the exponent n only shows a minor change. One should be cautious here to interpret the high shear fit viscosities η_∞ as real physical quantities.

Figure 6 shows the dependence of the MR effect for a shear rate of 28 s^{-1} on the magnetic induction. In the carbonyl iron case a quadratic dependence is observed,

$$\Delta\tau(B) \approx c_B B^2 \quad , \tag{13}$$

the pre-factor c_B having a value of $8.0\cdot10^4$ Pa/T^2. Some of the experimental values are listed in Table 3 for comparison. For inductions of 0.3 T and 0.4 T it was neces-

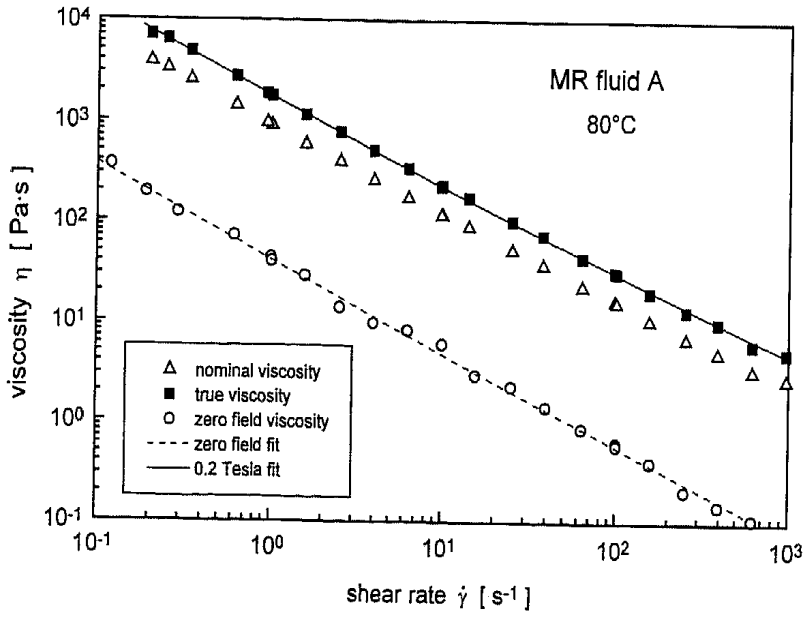

Fig. 5 Viscosity function of the carbonyl iron MR fluid A at 80 °C without field (circles) and at a magnetic induction of 0.2 Tesla (full squares)

Table 3 Experimental values measured with the 2×90°-cup DS09EB2 on MR fluid A at a shear rate of 28 s^{-1} and 80 °C

Magnetic induction B^* [T]	Apparent viscosity $\bar{\eta}$ [Pa s]	True viscosity $\eta(B)$ [Pa s]	Viscosity ratio $\eta(B)/\eta(0)$	Shear stress $\tau(B)$ [Pa]	MR effect $\Delta\tau(B)$ [Pa]
0	2.1	2.1	1	59	0
0.1	18.5	34.9	≈17	977	≈920
0.2	58.7	115	≈55	3230	≈3200
0.3	128*)	254	≈120	7110	≈7100
0.4	232**)	462	≈220	12900	≈12900

*) H = 4.5 mm, torque factor 2
**) H = 3 mm, torque factor 3

sary to reduce the effective height of the rotor in the gap to reach the high shear stress values.

Figure 7 demonstrates the evaluation of the viscosity at $B^* = 0.2$ T for nano MR fluid C at 25 °C. Without field (full diamonds) a viscosity plateau is reached at high shear rates (broken line). With field the shear rate sweep of the Physica rheometer only reaches 64 s^{-1} due to the torque limit. The parameters of the full line are $\tau_0(B) = 356$ Pa, $\eta_\infty(B) = 0.012$ Pa s, $n(B) = 0.129$.

The dependence of the MR effect on the magnetic induction is shown in Fig. 8. In contrast to the carbonyl iron sample no simple quadratic dependence is observed. At low induction values higher MR effects are observed compared to sample A in Fig. 6 (e.g. 1000 Pa for MR flu-

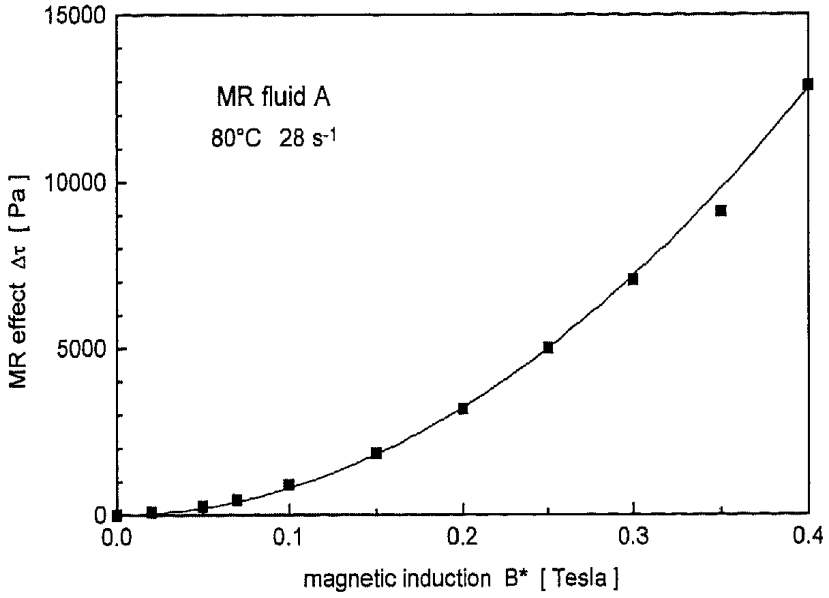

Fig. 6 Dependence of the MR effect of MR fluid A on the magnetic induction for 80 °C and a shear rate of 28 s^{-1}

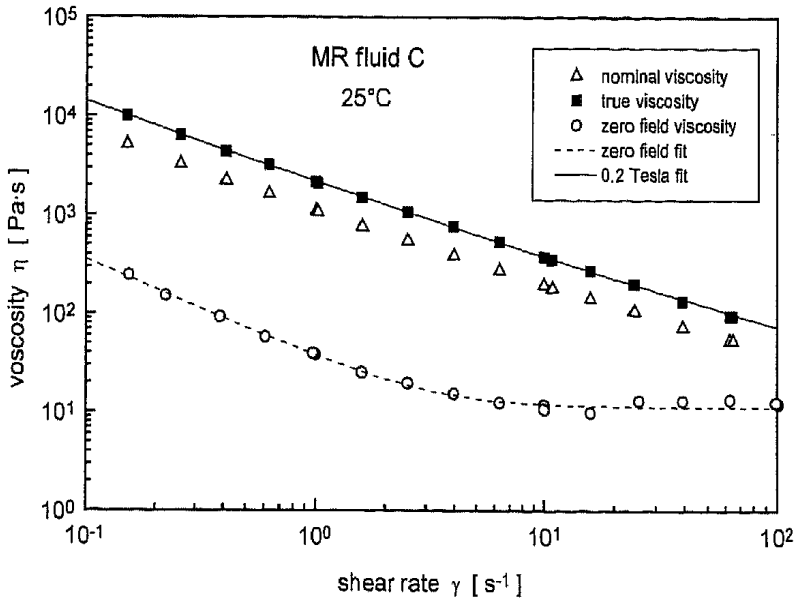

Fig. 7 Viscosity function of the nano MR fluid C at 25 °C without field (circles) and at a magnetic induction of 0.2 Tesla (full squares)

id A compared to 3300 Pa for MR fluid C at 0.1 T). At 0.1 to 0.2 T $\Delta\tau$ increases approximately linear with B. At still higher inductions the MR effect will reach a saturation plateau (Kormann et al., 1994) which is generally smaller than that of a carbonyl iron MR fluid at the same solid content.

Magnetic properties of the fixtures

The magnetic inductions B^* given above are nominal values measured by means of a hall probe (F. W. Bell Gauss meter model 9500) located in the middle of the gap without MR sample in the test fixture (compare Appendix II). Figure 9 shows the magnetic induction B^* measured in the 2×90°-cup DS09EB2 as a function of the coil current of the external electromagnet (1350 windings of an rectangular copper wire of 1 mm×3 mm) having a cross-section of the soft iron yoke of 1600 mm^2 outside the test fixture. The minimal cross-section of the yoke is 34 mm^2 right in the center of the test fixture (compare Fig. 2). A linear increase of B^* is found nearly up to 0.3 T (0.1 Tesla (T) = 1 kGauß) or 1.8 A. For higher currents the magnetic flux density is limited by the saturation magnetization of the yoke. When the coil current was switched off again a remaining induction of less than 4.510^{-4} T was measured in the gap indicating that remanence was negligible.

Circumferential field distribution (2×90°cup)

The hall probe had a thickness of 1 mm and a breadth of 4 mm. For the big 2×90°-cup DS20EB1 it was possible to have a closer look on the homogeneity of the magnetic flux density in the gap by placing the probe at various locations in the test fixture for a nominal magnetic induc-

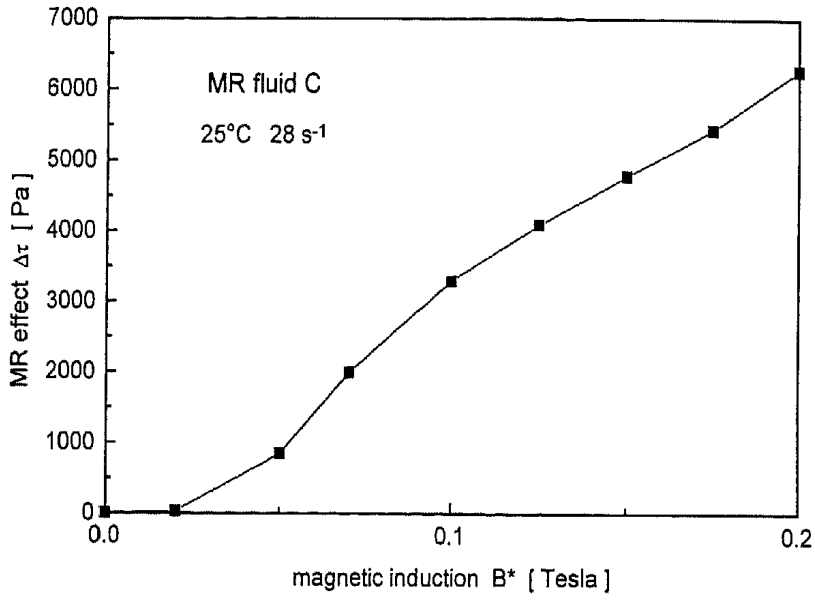

Fig. 8 Dependence of the MR effect of MR fluid C on the magnetic induction for 25 °C and a shear rate of 28 s^{-1}

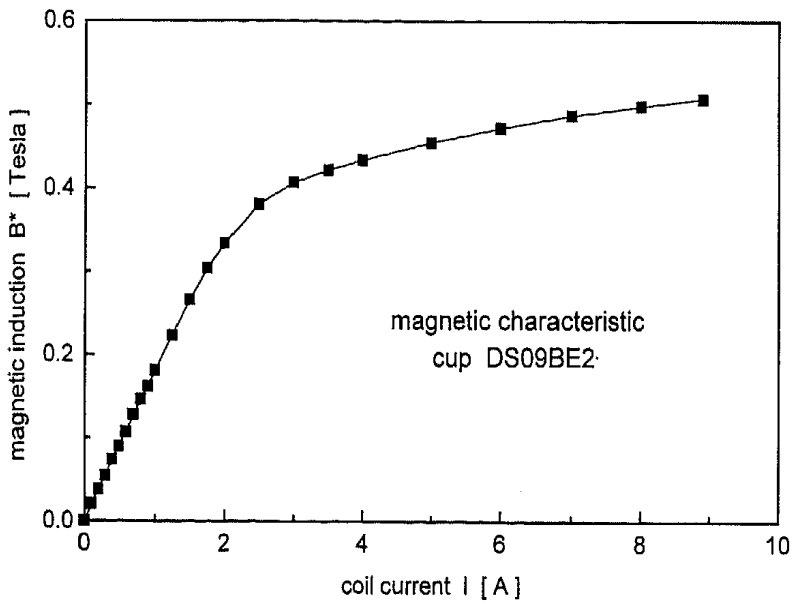

Fig. 9 Magnetic characteristic of the small 2×90°-cup DS09BE2 (compare Table 4) measured in the center of the gap

tion of 0.2 T. For the measurement as a function of the angle Θ the probe was put into contact to the inner wall of the annular gap (Fig. 10) the sensitive area being positioned approximately in the vertical center of the gap. As expected B^* is fairly constant up to 45°. However, due to stray fields the measured flux outside the soft iron sector is not negligible. At an angle of 50° the remaining induction is still about 25% of that in the gap of the iron yoke. Assuming zero field conditions for the sample outside the two 90° sectors (as done earlier and in Eq. (11)) can therefore only be a rough approximation.

A more realistic description would replace the nominal angle $2\times90° = \pi$ under field by an effective angle $\alpha(B)$. The latter is depending on the magnitude of the imposed magnetic flux density B. At small B most of the magnetic flux is guided within the yoke ($\alpha \cong \pi$) whereas at high B the small cross-section of the yoke in the center of the cup reaches saturation thus causing distinct stray fields ($\alpha > \pi$). In this case Eq. (11) has to be replaced by

$$\tilde{\tau}(B) = \frac{\alpha(B)\,\tau(B) + [2\pi - \alpha(B)]\,\tau(0)}{2\pi} \,. \qquad (11a)$$

By using Eqs. (11) and (12) the true magnetorheological effect is likely to be overestimated. It is outside the topic of this paper, however, to discuss this matter quantitatively.

Axial field distribution

The height dependence as investigated at an angle $\Theta = 0$ is shown in Fig. 11. A flux density overshoot is found near the corner of the yoke. In addition a non-negligible

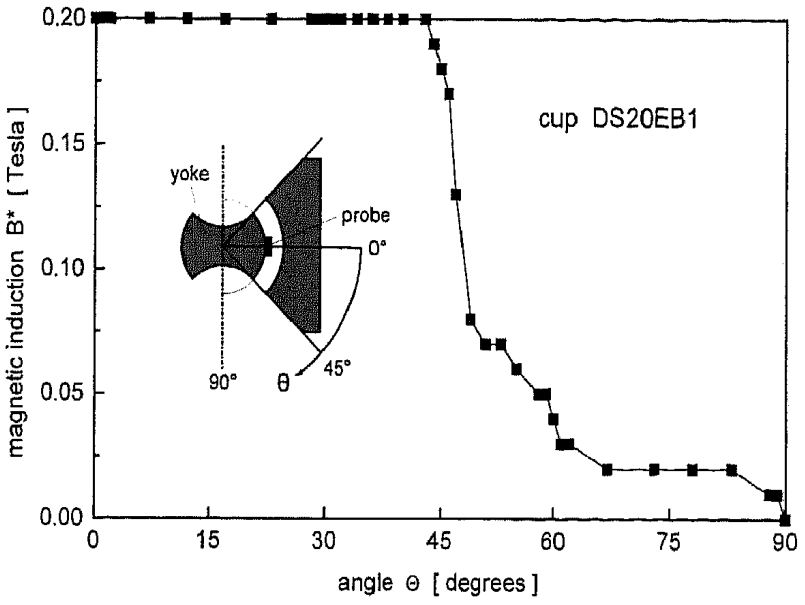

Fig. 10 Circumferential distribution of the magnetic induction for the big 2×90°-cup DS20EB1 (compare Table 4)

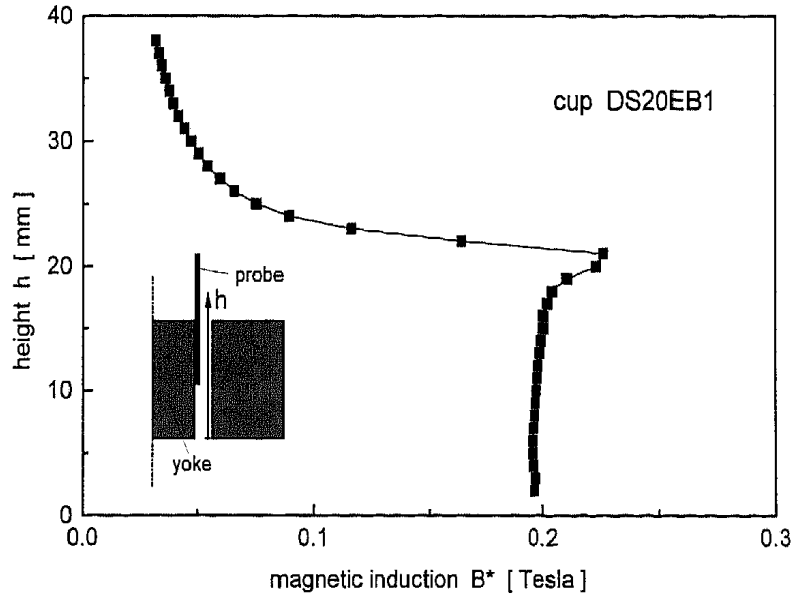

Fig. 11 Axial distribution of the magnetic induction for the big 2×90°-cup DS20EB1

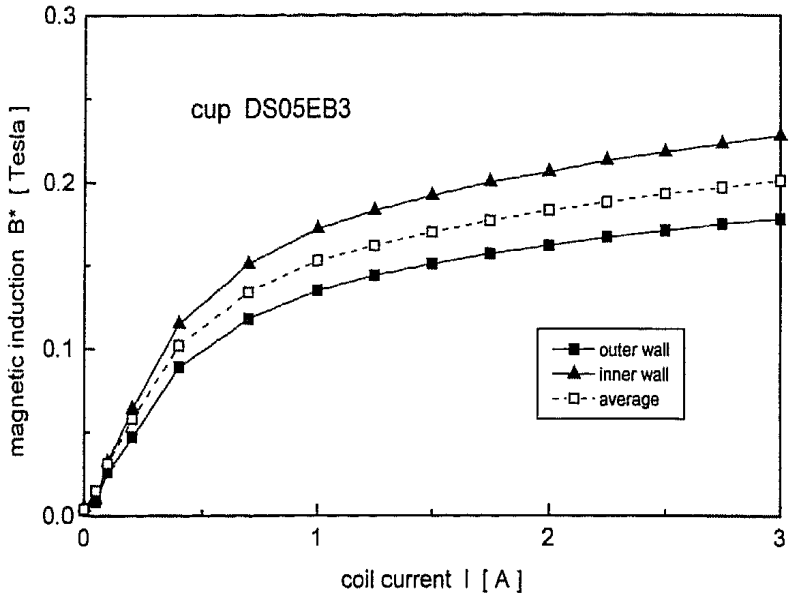

Fig. 12 Magnetic characteristic of the 360°-cup DS05EB3 measured for two radial positions of the hall probe

induction is measured above the shear gap ($h > 20$ mm). This indicates that part of the magnetic flux is bypassed above and below the soft iron yoke. The bypass has no influence on the measured torque, however. Similar effects as measured for cup DS20EB1 are to be expected for the fixtures with smaller gaps. No direct investigation was possible, though, with the available hall probe dimension.

Radial field gradient

It is also very important to take into account the radial flux density gradient in the gap which is due to a radial variation of the yoke cross-sectional area. For a demonstration we show in Fig. 12 the magnetic induction for a probe position at the inner gap wall (full triangles) and at the outer gap wall (full squares) of the 360°-cup DS05EB3. The induction increases approximately linear with the coil current up to about 0.1 T. The much smaller increase above that level indicates that the center yoke in the tool approaches saturation. Over the full range of the characteristic the flux density close to the inner wall is approximately 20% higher than that at the outer wall. If the finite thickness of the probe is taken into account this means that the total gradient across the gap could be in the order of about 30%. Note that the induction difference across the gap will increase with growing gap width. The nominal inductions B^* given in this paper correspond to the average of the two limiting curves (unfilled squares) which correspond to a probe location in the middle of the gap.

Table 4 lists values demonstrating the radial flux density gradient for the big (DS20EB1) and small (DS09EB2) 2×90°-cups at a nominal induction of 0.2 T measured in the middle of the gap without sample. The given radii represent the location of the center of the probe. According to the last column of Table 4 the measured radial induction gradient is in the order of 26% for the big cup and of 16% for the small cup. If the gap is subsequently filled with MR fluid B the resulting flux (at constant coil current) increases distinctly. The change is in the order of 20% for the big cup and only 4% for the small cup. Note that the flux density change due to the sample in a true measurement will be less that of Table 4 since during the test the presence of the rotor will reduce the amount of MR fluid in the gap.

Table 4 Magnetic inductions in the gap of two test fixtures measured without MR fluid and rotor for a nominal value of 0.2 Tesla and resulting change if the gap is filled with MR fluid B (hall probe thickness 1 mm) the coil current remaining constant

2×90°-cup	Radius [mm]	Sensor position	Induction B^* without MRF [Tesla]	Induction B with MRF [Tesla]	Flux density change due to MRF [%]	Radial gradient with MRF [%]
DS20EB1	15.5	inner wall	0.221	0.264	20	
	≈17.8	center	0.200			26
	20.0	outer wall	0.174	0.210	21	
DS09EB2	8.5	inner wall	0.217	0.223	3	
	≈8.9	center	0.200			16
	9.4	outer wall	0.185	0.193	4	

A comment is necessary for MR fluids that tend to sedimentation: The radial induction gradient causes a magnetic force on the pigment particles which drives them towards the inner yoke wall. If this occurs the concentration of pigment near the rotor wall will be less than the nominal solid concentration in the quiescent state. Too low viscosities will then be measured in concentric cylinder devices. The effect becomes the more important the bigger the magnetizable particles are.

Field variation due to magnetization of the MR fluid

For a discussion of the relation between the magnetic flux density without and with MR fluid in the gap we make use of the simple magnetic circuit depicted in Fig. 13. The field is created by the coil (I current, N number of windings) and transported to the shear gap by the yoke (l_Y length, μ_Y relative permeability). At the rheometer tool the magnetic flux passes through a gap of non magnetic material, e.g. air or non magnetic steel (l_G length, $\mu_G = 1$) and in part through the MR fluid (l_F length, μ_F relative permeability).

The magnetic induction B at the sample location (compare Appendix II) follows as

$$B = \mu_0 NI \left[l_G + \frac{l_F}{\mu_F} + \frac{l_Y}{\mu_Y} \right]^{-1} . \tag{14}$$

Without MR fluid in the gap we simply have to set $\mu_F = 1$ and obtain the value for B^*

$$B^* = \mu_0 NI \left[l_G + l_F + \frac{l_Y}{\mu_Y} \right]^{-1} . \tag{15}$$

For known values of μ_F and μ_Y the two equations enable in principle to calculate the flux change for a constant coil current. In the case $l_G \gg l_F + l_Y/\mu_Y$, which means the magnetic resistance of the path through the rotor material or non-magnetic steel dominates, this change will be small. This is the situation for cup DS09EB2. It should also be mentioned here that the insertion of the hall probe into the gap filled with MR fluid introduces an additional gap with $\mu = 1$ in the magnetic circuit.

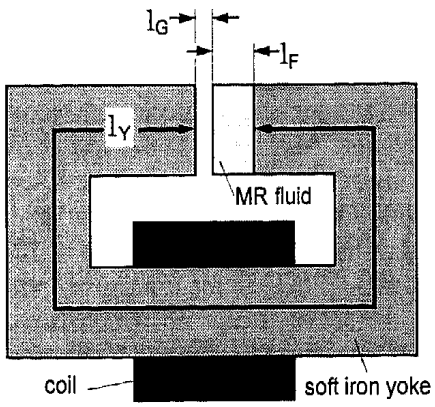

Fig. 13 Simple magnetic circuit (schematic)

As a result of the analysis of the magnetic properties of the test fixtures it must be said that a sound quantification of the effective induction during the measurements is not trivial. Due to the distinct gradients inherent in the yoke design one has to expect differences in the MR effects determined by different rheometers. Similar arguments hold of course for measurements on ER fluids. To our knowledge these problems have so far not adequately been addressed in the literature.

Comparison of MR data from the various concentric cylinder cups

To compare results from the three concentric cylinder cups, we show in Fig. 14 the zero field and the 0.1 T viscosity function of MR fluid B at 25 °C. The agreement of the zero field measurements from the three cups (broken line represents the fit by Eq. (10)) is satisfactory. The bigger scatter in the shear thinning regime is attributed to operating at the lower torque limit of the instrument. In this range frictional forces of the motor bearing play an important role. In addition, it must be said that the relatively small gap dimensions of cups DS09EB2 and DS05EB3 are sensitive to slight variations of the rotor concentricity and that due to the relatively small height of the shear gap edge effects are difficult to take into account correctly.

For the measurements under field the rheometer is operating in its upper torque limit such that frictional forces do not play a role. Except from the above mentioned edge effects we now have to take into account the errors in the effective magnetic induction as discussed in the preceding section. Yet an encouraging agreement is found. The full line represents the measurement with the small 2×90°-cup. The full circles give the data of a reproduction measurement. One of the two tests performed in the 360°-cup coincides nicely with the broken line whereas the reproduction run (full squares) lies below that at high shear rates. Only a very narrow shear rate range could be covered with the big 2×90°-cup (full triangles). These data are distinctly higher that those of the smaller cups. The likely reason is the larger shear gap width that gives rise to a much higher flux density increase due to the MR fluid (compare Table 4).

Figure 15 shows a comparison of the MR effect of the same sample as a function of the magnetic induction B^* as measured by using the different cups. For both the 2×90°-cup DS09EB2 and the 360°-cup DS05EB3 data from three independent measurements performed on different days are presented to judge the reproducibility of

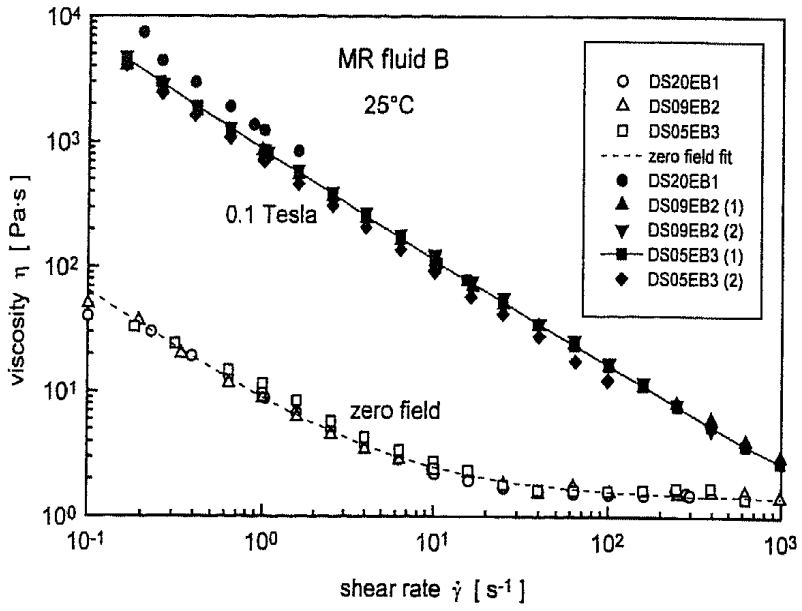

Fig. 14 Comparison of the zero field (unfilled symbols) and 0.1 Tesla (full symbols) viscosity functions of MR fluid B at 25 °C as measured by means of the three cups (numbers in brackets denote run no. in the case of a repetition of the measurement)

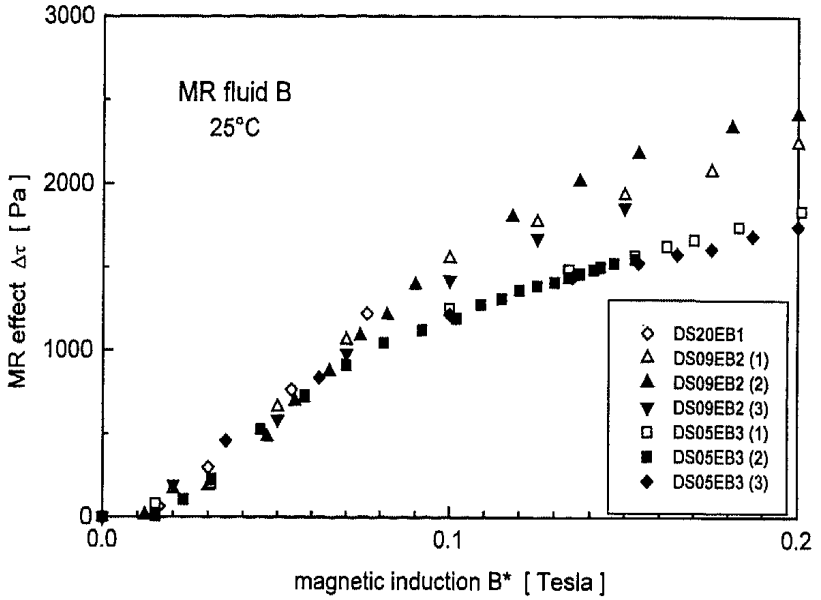

Fig. 15 Comparison of the dependence of the MR effect of MR fluid B at 25 °C on the magnetic induction as measured by means of the three cups (numbers in brackets denote run no. in the case of a repetition of the measurement)

the test results. In the low flux density range ($B^* < 0.1$ T) the data from various test geometries coincide with a scatter of about 100 Pa. Here, DS20EB1 gives the highest MR effect. For higher magnetic flux densities the small 2×90°-cup DS09EB2 yields systematically higher MR effects compared to the 360°-cup. The good reproducibility of the latter is noticeable. In this range an additional magnetorheological contribution to the torque due to stray fields outside the 90° sectors (compare Fig. 10) seems responsible for the higher values of the 2×90°-cup. This effect is expected to become more important when the soft iron in the center of the tool approaches saturation.

Dissipative heating

For high viscosity samples and shear rates approaching 1000 s^{-1} dissipative heating may become important. A simple method to check the temperature effect for a given tool design is to use a Newtonian fluid of known viscosity comparable to the MR fluids under consideration. In a step shear rate test a distinct temperature rise versus time would result in a gradual decrease of the viscosity reading. The latter yields an average temperature increase of the sample if compared to the temperature dependence of the calibration oil viscosity. If dissipative heating becomes distinct it may become necessary to only shear the sample for a short period and to use rest periods between the various shear rates for temperature re-equilibration.

We measured the apparent reduction of the viscosity of the calibration oil 10000 A (7.9 Pa s at 20 °C, 3.3 Pa s at 30 °C) in cup DS09EB2 for a nominal temperature of 20 °C using the shear rate sweep which is routinely used for characterizing the MR fluids (1 min for each shear rate). Due to dissipative heating the measured viscosity at the highest shear rate of 830 s^{-1} was only 3.4 Pa s which compares to an average temperature increase in the sam-

ple by about 10 °C. For shear rates 250 s^{-1} and 600 s^{-1} the estimated temperature rise was about 2° and 6 °C, respectively. In addition, for an MR fluid at 0.1 Tesla having a viscosity of 58 Pa s at 28 s^{-1} the sample temperature in the gap was measured by means of a thermocouple. After continuous shear of 10 min the temperature increase remained 0.4 °C.

High shear capillary viscometry (valve mode)

Slit die arrangement

Apparent shear rates up to 30000 s^{-1} as of interest for the application of MR fluids cannot be reached using conventional rotational rheometry. Here, it is advantageous to use the extrusion through a slit capillary. The distinct dissipation at high shear rates is not so severe in a capillary since most of the produced heat is continuously transported out of the capillary (forced convection). Figure 16 shows the design of the apparatus. The core unit is a rectangular slit of 0.4×4×20 mm attached to the barrel of a capillary rheometer. The flow rate is imposed by the speed of a piston and the extrusion pressure measured by a fluid pressure transducer. The slit die is located at the bottom of a block of non magnetic steel which contains boreholes to thermostat the block by means of a thermostat fluid (temperature range 0 ° up to 120 °C for the pressure transducers used). The upper part of the block is necessary to adapt the rectangular slit to the circular barrel. Equations (6) and (7) are used to evaluate the wall shear rate and stress, the pressure loss in the channel between slit die and pressure transducer being neglected. The cross-sectional view shows part of the yoke geometry of an electromagnet used to impose a magnetic induction perpendicular to the dominant plane of shear in the slit. The distance of the yoke tips on both sides of the slit is 4.5 mm. An induction of $B^* = 3.7$ T is measured for a coil current of 2 A. The onset of magnetic saturation occurs only at higher coil currents the maximal flux density being about 0.6 T.

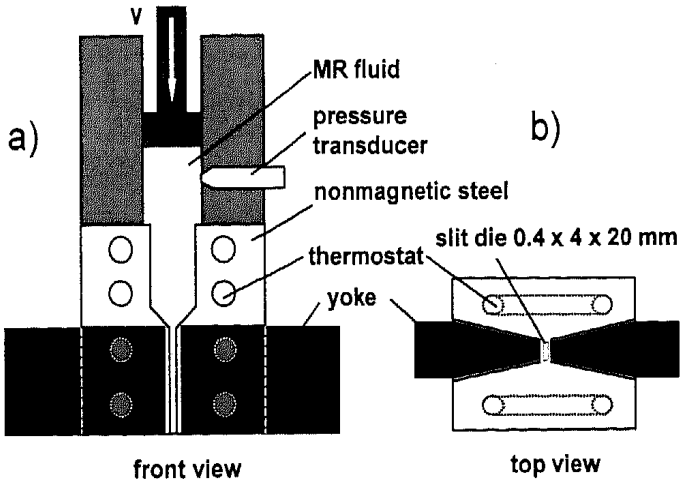

Fig. 16 Front view (a) and top view (b) of the slit die arrangement (schematic)

Experimental example

Measurements on MR fluid A at 25 °C are shown in Fig. 17 in a range of (apparent) shear rates 1100 to 38000 s^{-1} for inductions up to 0.4 T. The extrusion pressure covered was 0.5 to 15 bar. No correction for dissipative heating has been attempted since the data are considered to represent the sample performance (apparent viscosity function) in a throttle of similar geometrical design. Values for viscosity ratio and the MR effect for the shear rate 11400 s^{-1} are listed in Table 5.

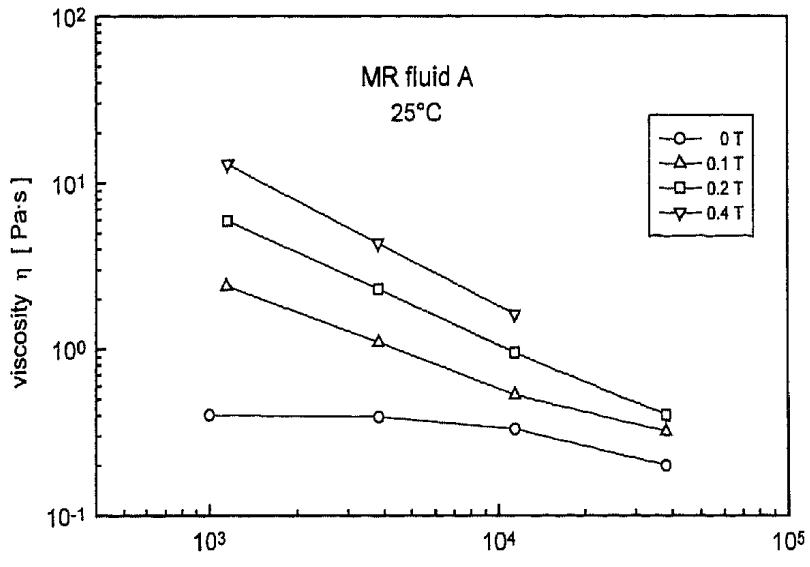

Fig. 17 High shear rate viscosity functions of MR fluid A at 25 °C and various magnetic inductions as measured by means of the slit die

Rheologica Acta, Vol. 35, No. 5 (1996)
© Steinkopff Verlag 1996

Table 5 Experimental values measured with the slit die on MR fluid A for an apparent shear rate of 11400 s^{-1} and 25 °C

Induction B [Tesla]	Viscosity η [Pa s]	Shear stress $\tau(B)$ [Pa]	Viscosity ratio $\eta(B)/\eta(0)$	MR effect $\Delta\tau(B)$ [Pa]
0	0.33	$3.8 \cdot 10^3$	1	0
0.1	0.53	$6.0 \cdot 10^3$	1.6	$2.2 \cdot 10^3$
0.2	0.95	$10.8 \cdot 10^3$	2.9	$7.0 \cdot 10^3$
0.4	1.62	$16.5 \cdot 10^3$	4.9	$12.7 \cdot 10^3$

Comparison of slit and concentric cylinder results

The capillary results may directly be compared with the concentric cylinder data for the overlapping (apparent) shear rate of 1000 s^{-1} (Table 6). The capillary data are by about 20% higher than those from the 2×90°-cup but give the same viscosity ratio. The higher value of the apparent viscosity from the slit die is most likely attributed to the neglected pressure drop in the tube between pressure transducer and the rectangular slit which also contains the entrance pressure loss into the slit die. A rigorous comparison of the slit and concentric cylinder results should also take into account the difference in dissipative heating (reduced in slit due to forced convection), stray field (2×90° geometry), flux density gradient across the sample (important for concentric cylinder), and time dependence of field. The latter is stationary for the 360° geometry, pulsating for the 2×90° geometry and yields a step-like onset at the entrance into the die.

Table 6 Comparison of slit die and concentric cylinder data (DS09EB2) on MR fluid A for an apparent shear rate of ≈1000 s^{-1} and 25 °C

Geometry	Shear rate $\dot{\gamma}$ [s^{-1}]	Viscosity $\eta(0)$ [Pa s]	Viscosity $\eta(0.2T)$ [Pa s]	Viscosity ratio $\eta(B)/\eta(0)$
slit die	1150	0.39	5.9	15.1
2×90°-cup	1000	0.31	4.9	15.8

Conclusions

Our study has shown that the 360° concentric cylinder geometry is the preferred method to measure magnetorheological properties of the MR fluids in the range of small shear rates. This method only requires a relatively small amount of sample (≈40 ml) to obtain the characteristic data necessary for development and rapid screening of MR fluids. The range of accessible shear rates is from less than 0.1 up to about 1000 s^{-1}.

Measurements using various geometries show that the zero field viscosity is accurate in the range ±15%. This error is valid for the Physica Rheolab MC 20 and our test geometry. Better results should be obtainable by a more accurate instrument with improved bearing of the rotating shaft.

The MR effect calculated from various measurements is found to be reproducible in a range of ±15% for 0.1 T magnetic flux density. At 0.2 T the 2×90° geometry yields consistently higher (+30%) values than the 360° geometry, mainly due to stray fields. It was demonstrated that a sound quantification of the effective flux density during the measurements is not trivial. Due to the distinct induction gradients inherent in the yoke design one has to expect differences in the MR effects determined by different rheometers. To our knowledge these problems have so far not adequately been addressed in the literature.

The 2×90° geometry offers more flexibility in terms of temperature range (≈0°...+150 °C) and ease of accessing high magnetic flux densities up to 0.5 T by means of an external electromagnet. Drawbacks are the flux density dependent stray fields that complicate the evaluation of the true MR effect as well as the pulsating field seen by rotating volume elements.

In combination with a commercial rotational rheometer both geometries enable to use standard types of tests, e.g. shear rate sweep or time sweep, that run automatically on the instrument. When operating at high shear rates both concentric cylinder geometries tend to be sensitive to dissipative heating. In this case high shear rates should only be applied for a short time (<1 s).

Though versatile, the rotational rheometers operate far outside the range of shear rates relevant for practical applications of the MR fluids. Design data for MR dampers and clutches can be obtained by slit rheometry. One instrument of this type applicable for shear rates up to 40000 s^{-1} has been described. The comparison of slit and 2×90°-cup results for a shear rate of about 1000 s^{-1} gave an encouraging agreement of about ±15% which is remarkable when various sources of systematic error are taken into account.

Due to forced convection dissipative heating is kept small. Also the time during which the fluid is submitted to the field is short. This is of advantage for MR fluids that tend to sedimentation in a magnetic field gradient. The drawback is the need for larger amounts of sample (≈0.1 L) and the more tedious mode of operation. Magnetic field gradients at the die exit may cause problems to collect the extruded sample completely in a beaker.

Acknowledgments The authors are indebted to I. Ulmerich and P. Schuler for the construction and development of the test tools. P. Schweizer is thanked for performing the concentric cylinder measurements and D. Lingenfelder for the slit die results. The help of G. Schmidt in preparing the figures is gratefully acknowledged.

Appendix I

Shear rate and stress in double concentric cylinder geometry

The notation is depicted in Fig. 3. For a Newtonian fluid the radial shear rate profile in the gap between a stationary and a rotating wall (R_i inner radius, R_o outer radius, $\beta \equiv (R_i/R_o)^2$) is given by (see e.g., Macosko, 1994)

$$\dot{\gamma}(r) = 2\frac{R_i^2}{r^2}\frac{\Omega}{1-\beta}\,, \tag{A1}$$

where Ω represents the relative angular velocity. For the double concentric cylinder tool we are interested in the shear rates at the rotor. Equation (A1) yields for the shear rate $\dot{\gamma}_1$ in the inner gap at the rotor wall ($r = R_{o1}$)

$$\dot{\gamma}_1 = \frac{2\beta_1\Omega}{1-\beta_1} \quad \beta \equiv \left(\frac{R_{i1}}{R_{o1}}\right)^2 \tag{A2}$$

and for the shear rate $\dot{\gamma}_2$ in the outer gap at the rotor wall ($r = R_{i2}$)

$$\dot{\gamma}_2 = \frac{2\Omega}{1-\beta_2} \quad \beta_2 \equiv \left(\frac{R_{i2}}{R_{o2}}\right)^2 . \tag{A3}$$

The preferred geometry is to make the apparent shear rates on both sides of the rotor equal to a shear rate $\dot{\gamma}$

$$\dot{\gamma} = \dot{\gamma}_1 = \dot{\gamma}_2 = \dot{\gamma}_z\,, \tag{A4}$$

where $\dot{\gamma}_z$ stands for the shear rate of the Physica Z-cup ($\beta = 0.850$). For a constant shear rate on both sides of the rotor the resulting shear stresses τ are equal, too. Thus the resulting torque M is simply given by

$$M = M_1 + M_2 = 2\pi\tau H(R_{o1}^2 + R_{i2}^2)\,. \tag{A5}$$

which yields for the shear stress Eq. (9).

Appendix II

Simple magnetic circuit

The magnetic flux density in the shear gap of a rheometer is derived for the simple magnetic circuit depicted in Fig. 13. The field created by the coil (I current, N number of windings) and transported by the yoke (l_Y length, A_Y cross-sectional area, μ_Y relative permeability) also passes through a gap of non-magnetic material (l_G length, A_G cross-sectional area) and through the MR fluid (l_F length, A_F cross-sectional area, μ_F relative permeability). The property of interest is the total magnetic flux Φ which is constant throughout the whole magnetic circuit if stray fields are neglected. The magnetic flux is given by (e.g., Joos, 1959)

$$\Phi = \frac{NI}{R_m} \quad [\mathrm{Vs}]\,, \tag{A6}$$

where R_m stands for the total magnetic resistance, the sum of the magnetic resistances of the yoke, gap, and sample, R_Y, R_G, and R_F, respectively:

$$R_m = R_Y + R_G + R_F\,. \tag{A7}$$

The various resistances are calculated as ($\mu_0 = 1.26 \cdot 10^{-6}$ Vs/(Am))

$$R = \frac{1}{\mu\mu_0 A} \quad \left[\frac{\mathrm{Vs}}{\mathrm{A}}\right]. \tag{A8}$$

Note that $\mu_G = 1$ and μ_Y and μ_F depend in general on the flux density. For a constant cross-sectional area along the magnetic circuit the magnetic flux density or magnetic induction B [$\mathrm{Vs/m^2}$ = Tesla (T)] at the sample location finally follows as

$$B \equiv \frac{\Phi}{A} = \mu_0 NI\left[l_G + \frac{l_F}{\mu_F} + \frac{l_Y}{\mu_Y}\right]^{-1}. \tag{A9}$$

The magnetic induction B is related to the applied magnetic field H [A/m] and magnetization $\tilde{M}$ [A/m] by (e.g., Statton, 1941)

$$B = \mu_o\,[H + \tilde{M}]\,. \tag{A10}$$

The advantage of using B to quantify the field is that the flux density does not exhibit jumps (if stray fields are neglected) in going from one material into another.

Rheologica Acta, Vol. 35, No. 5 (1996)

References

Ambacher O, Odenbach S, Stierstadt K (1992) Rotational viscosity in ferrofluids. Z Phys B – Condensed Matter 86: 29–32

BASF (1995) Nano-MR fluids, information brochure by BASF Aktiengesellschaft. Ludwigshafen, Germany, April

Bonnecaze RT, Brady JF (1992) Yield stresses in electrorheological fluids. J Rheol 36:73–115

Carlson JD (1994) The promise of controllable fluids. In: Borgman H, Lenz K (eds) Proc Actuator 1994. Axon, Bremen, p 261–270

Hartsock DL, Novak RF, Chaundy GJ (1991) ER fluid requirements for automotive devices. J Rheol 35:1305–1326

Hess S, Schwarzl JF, Baalss D (1990) Anisotropy of the viscosity of nematic liquid crystals and of oriented ferrofluids via non-equilibrium molecular dynamics. J Phys, Condens Matter 2:SA 279–284

Hess S, Weider T (1993) Report to BASF. Investigations on the structure and rheology of ferro-fluids. February

Janocha H, Rech B (1994) Measurements of MR fluids using rotational viscometers. Rheology 4:198–203

Joos G (1959) Lehrbuch der Theoretischen Physik, 11. Aufl. (Akademische Verlagsgesellschaft, Frankfurt)

Kamiyama S, Koike K, Wang Z-S (1987) Rheological characteristics of magnetic fluids. JSME Int J 30(263):761–766

Laun HM, Korman C, Willenbacher N (1996) Rheometry on MR fluids. II. Oscillatory shear investigations and effect of alternating fields, to be submitted to J Rheol

Kashevskii BE, Kordonskii VI, Prokhorov IV, Demchuk SA, Gorodkin SR (1990) Relaxation of viscous stresses in magnetorheological suspensions. Magnetohydrodynamics (USA) 26(2):140–148

Kordonsky VI, Shulman ZP, Demchuk SA, Prokhorov IV, Zaltsgendler EA, Khusid BM (1990) J Magn Magn Mater 85: 114–120

Kordonsky WI, Gorodkin SR, Medvedeva EV First experiments on magnetoelectrorheological fluids (MERFs) (1994) In: Tao R, Roy GD (eds) Electrorheological Fluids: Mechanisms Properties, Technology and Application. World Scientific, Singapore, pp 22–36

Kormann C, Laun M, Klett G (1994) Magnetorheological fluids with nano-sized particles for fast damping systems In: Borgmann H, Lenz K (eds) Proc Actuator 1994. Axon, Bremen, p 271–274

Lemaire E, Bossis G (1991) Yield stress and wall effects in magnetic colloidal suspensions. J Phys D 24:1473–1477

Minagawa K, Watanabe T, Munakata M, Koyama K (1994) A novel apparatus for rheological measurements of electromagneto-rheological fluids. J Non-Newtonian Fluid Mechanics 52:59–67

Macosko ChW (1994) Rheology – Principles, Measurements, and Applications. VCH Publishers, Weinheim New York Cambridge

Rabinow J (1948) The magnetic fluid clutch. AIEE Transactions 67: 1308–1315

Rosensweig RE (1985) Ferrohydrodynamics. Cambridge University, New York

Rosensweig RE, Kaiser R, Miscolczy G (1969) Viscosity of magnetic fluids in a magnetic field. J Coll Interface Sci 29(4):680–686

Skjeltorp AT (1984) Colloidal crystals in magnetic fluid. J Appl Phys 55(6): 2587–2588

Statton JA (1941) Electromagnetic Theory. McGraw-Hill, New York

Tönshoff HK, Stegmann A (1995) ERF/MRS Based Precision Linear Drive System, to be published in the Proceedings of the Fifth Conference on Electrorheological Fluids, Magnetorheological Suspensions and Related Technology, Sheffield, UK, 10–14 July

Weiss KT, Carlson J, Nixon DA (1994) Viscoelastic properties of magneto- and electro-rheological fluids. J Intelligent Mat Systems & Structures 5:772–775

Weser T, Stierstadt K (1985) Magnetoviscosity of concentrated Ferrofluids. Z Phys B – Condensed Matter 59:257–260